

Molecular Insights on the Interference of Simplified Lung Surfactant Models by Gold Nanoparticle Pollutants

SHEIKH I. HOSSAIN¹, NEHA S. GANDHI², ZAK E. HUGHES³, Y. T. GU⁴, SUVASH C. SAHA^{1*}

¹School of Mechanical and Mechatronic Engineering, University of Technology Sydney, 81 Broadway, Ultimo NSW 2007, Australia

²School of Mathematical Sciences, Queensland University of Technology, 2 George Street, GPO Box 2434, Brisbane QLD 4001,

³School of Chemistry and Biosciences, The University of Bradford, Bradford, BD7 1DP, UK

⁴School of Chemistry, Physics & Mechanical Engineering, Queensland University of Technology, 2 George Street, GPO Box 2434, Brisbane QLD 4001,

*corresponding author: suvash.saha@uts.edu.au

Abstract

Inhaled nanoparticles (NPs) are experienced by the first biological barrier inside the alveolus known as lung surfactant (LS), a surface tension reducing agent, consisting of phospholipids and proteins in the form of the monolayer at the air-water interface. The monolayer surface tension is continuously regulated by the alveolus compression and expansion and protects the alveoli from collapsing. Inhaled NPs can reach deep into the lungs and interfere with the biophysical properties of the lung components. The interaction mechanisms of bare gold nanoparticles (AuNPs) with the LS monolayer and the consequences of the interactions on lung function are not well understood. Coarse-grained molecular dynamics simulations were carried out to elucidate the interactions of AuNPs with simplified LS monolayers at the nanoscale. It was observed that the interactions of AuNPs and LS components deform the monolayer structure, change the biophysical properties of LS and create pores in the monolayer, which all interfere with the normal lungs function. The results also indicate that AuNP concentrations >0.1 mol % (of AuNPs/lipids) hinder the lowering of the LS surface tension, a prerequisite of the normal breathing process. Overall, these findings could help to identify the possible consequences of airborne NPs inhalation and their contribution to the potential development of various lung diseases.

Keywords: Lung surfactant; Gold nanoparticles; Surface tension; Coarse-grained molecular dynamics; Lipid monolayers

1. Introduction

Research on nanoparticles (NPs) in biological sectors has been driven by significant applications in the fields of nanomedicine, drug delivery, disease detecting and bio-sensing [1-4]. While NPs have the potential to advance new technologies, prior studies have also demonstrated their potential risk to human health. One such health risk is the uptake of airborne NPs [5-7], where the interaction of NPs with the lungs can alter the normal mechanical properties of lung components during breathing. The probability of inhaling airborne particles is mostly determined by the particle size, with small particles (e.g. particles <100 nm in diameter) more likely to be inhaled deeply into the lungs, where they may penetrate the epithelium and enter the bloodstream [8]. Regular inhalation of airborne NPs intensifies the probability of lung ageing, promoting lung malfunction, and can induce serious lung diseases such as asthma, lung cancer, acute respiratory distress syndrome, and more [8, 9]. The inhaled NPs interact with the lung surfactant monolayer (LS), the first biological barrier inside the lung alveolus, and may cause serious damage in the surfactant layer [6, 10, 11]. Furthermore, in experimental studies, it was found that the inhaled NPs may interact with the surfactant components, inhibit normal lung functioning and induce lung diseases [12, 13]. As such, molecular level research that can explore the structural changes in the LS caused by the inhaled NPs, and help trace out the adverse effects of these NPs on the usual lungs activities, is required [14].

LS is mainly composed of phospholipids (saturated and unsaturated), cholesterol and a small number of proteins (approximately 90% lipids and 10% proteins by weight), which together form a stable monolayer at the air-water interface inside the alveolus [15, 16]. About half of the lipids consist of dipalmitoylphosphatidylcholine (DPPC) [16], a saturated phospholipid, which can be packed tightly in the monolayer at physiological temperature and facilitates the LS monolayer the ability to reach a surface tension of ~0 mN/m, without collapsing, during compression [17]. Other surfactant lipids, including the unsaturated phospholipid palmitoyl-2-oleoyl-sn-glycero-3-phosphoglycerol (POPG), fluidize the monolayer and are thought to enhance resspreading [18]. During breathing, the alveolus surface area repeatedly expands and compresses, LS serves to attain ~20-25 mN/m equilibrium surface tension [19] at the air-water interface while the alveolus expands.

Experimental [17] and computational studies [20-22] have provided information on the various biophysical phenomenon of LS monolayers such as phase behaviour change, surface tension,

surface pressure, the area per lipid (APL), LS components density, *etc.* An increasing number of studies based on molecular dynamics (MD) simulations have found that the LS monolayer at the air-water interface changes to the liquid condensed (LC) phase from the coexistence of LC and liquid expanded (LE) phases [23] as the APL decreases to ~0.46-0.47 nm² from ~0.49-0.55 nm² [21]. Similarly, the surface tension of the monolayer, which is directly proportional to the APL [24], reaches an equilibrium value of ~23 mN/m during inhalation and reduces to ~0 mN/m in the LC phase upon exhalation. The major LS component, DPPC, undergoes a phase change from the coexistence of liquid expanded and condensed phases (LE+LC) to LC phase at ~41°C. The unsaturated lipids present in LS typically have a lower phase transition temperature than the saturated lipids, and so remain in a LE phase at a physiological temperature [25].

Computational studies can aid in the understanding of the interaction between the surfactant and NPs by providing insights into the molecular level behaviour. Coarse-grained molecular dynamics (CGMD) simulations have been applied to explain the structural and molecular changes in LS due to the inhalation of different types of NPs, for example, carbon nanotubes [10, 11, 26], fullerene [6, 7, 27], graphene [28-30], silica [31], and others [2, 14, 32-34]. In addition, the interaction of LS monolayer with other molecules has been investigated, e.g. benzo[a]pyrene [35], antimicrobial peptides [36] and prednisolone [37] by CGMD simulations. The effects of NP size [2, 14, 27, 38], shape [14, 32], concentration [6, 7, 27, 37] and surface charge [33, 39, 40] have been considered. In LS monolayer, it was reported that the aggregation of larger fullerene NPs (C₅₄₀) in the monolayer reduced the monolayer surface tension unlike the smaller fullerene NPs (C₆₀) [27]. It was reported that small hydrophilic NPs (<5 nm) could quickly penetrate the LS layer [2] regardless of the NPs shape and LS surface tension [14]. A negligible side effect (less disruption in LS monolayer) with the highest penetration ability was found for the rod shape hydrophilic NPs [32] while hydrophobic and charged NPs could become trapped in the LS monolayer [33].

Gold nanoparticles (AuNPs) have potential applications in bio-imaging, disease detection, drug delivery, and diagnostic purposes due to their biocompatibility, low-toxicity, and easy translocation properties [1, 3, 4]. In experimental studies, AuNPs are commonly used as a drug delivery agent after modifying their surfaces by the attachment biomolecule ligands [12, 41-43]. In parallel with experimental studies, modelling studies have shown considerable interest

in the use of AuNPs, investigating their toxicity [44], size [38, 45], shape [46] and surfaces modification [47, 48].

Excessive exposure to AuNPs may cause serious problem to human health, and the possible health effects of AuNPs are a continuing concern to the nanotechnology industry [49]. With the increased use of AuNP containing consumer products, the potential for an individual's exposure has also increased [50]. Goldsmiths and workers employed in gold mining and refining are likely to inhale gold dust [51-53], and the toxic effect of AuNPs by inhalation in animal models has been studied [50, 54]. Based on the emerging evidence on the toxicity of gold particles, the National Institute of Standards and Technology (NIST) has suggested the use of AuNP as a model system for nanotoxicological research [55]. Moreover, different experimental, medical and survey studies have shown that AuNPs can disrupt routine lungs functions and promote respiratory diseases [12, 13, 51, 52]. However, relatively few studies have investigated the interaction between human biological components and bare AuNPs [12, 13, 56].

In a recent experimental study, it was postulated that the engineered NPs like AuNPs have potential similarities to the environmental NPs (most of the environmental NPs are treated as pollutants) [54]. Therefore, the findings regarding the effects of AuNPs (as pollutants) may be relevant to understanding the effects of other nano-pollutants on lungs. For instance, the observed effects of spherical and hydrophobic AuNPs on model surfactant, such as pore formation, lipid packing disturbance, and inhibition of some biophysical properties, may also be applicable to understanding effects of other spherical hydrophobic NPs [6, 7, 57].

The experimental paper, Bakshi *et al.* [12], whose work we have based our study around, have also reported AuNPs as model pollutants. The authors measured the surface activity of the surfactant membrane using a captive bubble tensiometer and reported that AuNPs lower the surface activity of the LS system during the breathing cycles. The authors proposed that bare AuNPs hinder the reduction in the surface tension value during the compression process. The findings of Bakshi *et al.* [12] are in agreement with the results of Zhang *et al.* [13] on the interaction of bare AuNPs with DPPC enriched LS monolayer. However, to the best of our knowledge, no computational studies on bare AuNPs interacting with LS monolayer have been reported to support the experimental hypothesis.

Recent computational studies [33, 58] have highlighted that the LS proteins adsorb quickly on the NP surface and mediate the protein corona formation by directly interacting with lipids. In this study, we only considered simplified monolayers consisting of lipids and cholesterol. The molecular level interactions between bare AuNPs (as model pollutants) and the simplified LS monolayer components were investigated using CGMD simulations. We used spherical hydrophobic AuNPs with a diameter of ~3 nm and concentrations of ~0.1, ~0.9, ~1.56 and ~3.52 mol % of AuNPs/lipids. AuNP has specific properties such as chemical composition, nano-aggregation, the lattice constant, and potential. These properties provide unique attributes as compared to other hydrophobic NPs [7, 59, 60]. To our knowledge, there is no literature available on the modelling of bare AuNPs varying in concentrations with LS monolayer and this will be the first study to provide insight into biophysics of AuNPs interaction with LS monolayer. The simulation results will pave the way to rationalize how AuNPs could impede the normal pulmonary functions and could damage the lung alveoli by pore formation and nano-aggregation in molecular scale.

2. Computational methods

MD simulations were performed on a number of systems, each consisting of a water layer bounded by two symmetric lipid monolayers at the vacuum-water interface (Fig. 1a and Fig. S1a). The systems were prepared using a similar procedure as described by Baoukina *et al.* [61] and Estrada-López *et al.* [37]. Two different LS lipid mixtures (DPPC:POPG and DPPC:POPG:CHOL), separated by 6 nm of water, were used to build two different systems. Several experimental studies have reported that higher amounts of cholesterol (>40 mol % or ~20 % wt/wt) greatly decrease the ability of LS to attain low surface tension, whereas physiological levels of cholesterol enhance the adsorption of surfactant phospholipids to the surface tension of ~0 mN/m [62]. Therefore, we have considered monolayers consisting of 10 mol % (~5% wt/wt) cholesterol in this study, consistent with physiological levels. Two systems with these lipid compositions were built, and single AuNP was placed close to the upper (vacuum) side of one monolayer only. A separate set of systems (Table 1) were prepared by placing the AuNPs onto both monolayers, consisting of DPPC:POPG:CHOL, separated by 21 nm of water. In these systems, different concentrations of AuNPs were used to explain the mechanism of LS monolayer perturbation by the AuNPs concentrations.

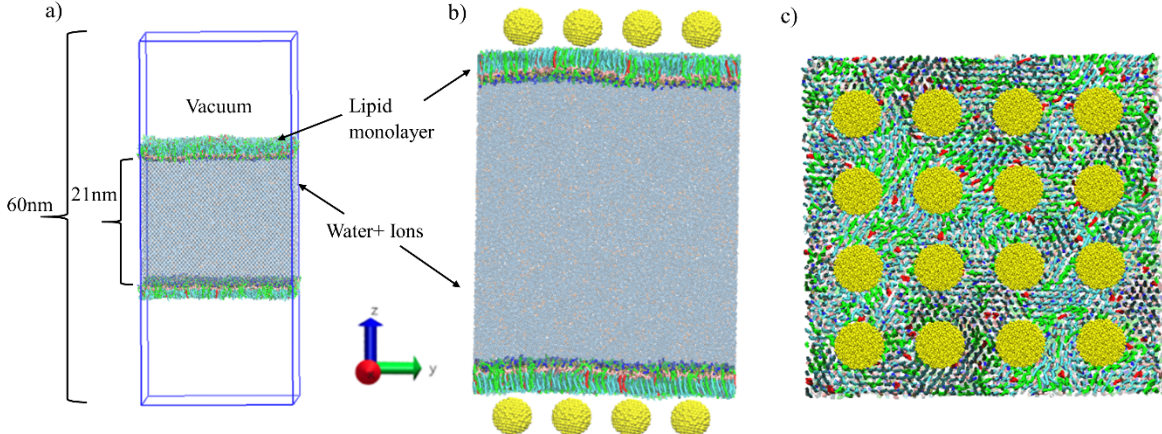


Fig. 1. The initial structure of model LS monolayer at the vacuum-water interface. (a) System configuration without AuNPs, (b) side view of the system with ~ 1.56 mol % of AuNPs/lipids, and (c) top view to the upper monolayer with ~ 1.56 mol % of AuNPs/lipids.

2.1. Simplified lung surfactant model

The bilayer systems DPPC:POPG (7:3) and DPPC:POPG:CHOL (7:3:1) were built using an INSANE [63] script with 1023 phospholipids in each monolayer. The two monolayers were prepared by separating two leaflets of a bilayer. The plane of the monolayers was parallel with the XY plane of the system. A water box ($25\text{ nm} \times 25\text{ nm} \times 6\text{ nm}$) was placed between the two monolayers and filled with ~ 26000 CG water beads. Then, the whole system was embedded in a periodic boundary box ($25\text{ nm} \times 25\text{ nm} \times 60\text{ nm}$) such that the two monolayers were separated by a water layer and $\sim 50\text{ nm}$ of vacuum (Fig. S1a). These systems were extended to NP-based DPPC:POPG and DPPC:POPG:CHOL systems (Table S1) where a single AuNP was placed in the vacuum about 6 nm above one monolayer. In addition, a small control system DPPC:POPC (7:3) was prepared in accordance with the Estrada-López *et al.* studies [37] to validate all other LS systems (Table S1). The lipid order parameter values of the control system were considered for comparison with Estrada-López *et al.* studies [37]. Comparison of the control system APLs and order parameters (supplementary information) with previously published results confirm that the choice of model/simulation parameters used do not introduce any artefacts.

To study the effects of NP concentration, we also built another system consisting of the mixture of DPPC:POPG:CHOL (7:3:1) using the method mentioned above. Here, the two monolayers were separated by $\sim 21\text{ nm}$ of water and $\sim 34\text{ nm}$ of vacuum in a box of dimension $25\text{ nm} \times 25\text{ nm} \times 60\text{ nm}$, as shown in Fig. 1. Different *in vivo*, *in vitro* and *in silico* studies have suggested

that a thickness of liquid-layer ranging from 0.025 to 5 μm may have a significant impact on surfactant molecule transport during LS monolayer collapse [64]. A thinner liquid layer may slow surfactant molecule transport and thereby help to increase the resistance of LS to monolayer collapse [64]. We have used ~21 nm water layers as a compromise between computational cost and larger system size. Each monolayer contained 1023 lipid molecules while the water slab contained about ~96,000 water beads. An ionic concentration of 150 mM NaCl was added to the water slab. Due to the negative charge on the POPG phospholipid head group, an equal number of water beads were replaced by positive ions (Na^+) beads to make the systems electro-neutral.

The DPPC:POPG:CHOL monolayer systems (Table 1) were first equilibrated (500 ns) in the absence of any NPs at volumes corresponding to two different APLs, 0.46 and 0.53 nm^2 , relating to the monolayer compression and expansion states, respectively. Once the monolayers had been equilibrated, the systems containing the AuNPs present were constructed by placing AuNPs in the vacuum space in close proximity (<1 nm) to the lipid tails of the monolayers. Concentrations of AuNPs of ~0.1, ~0.9, ~1.56 and ~3.52 mol % were simulated (here mol % was calculated as the % of molecules with respect to the total number of lipid and NP molecules).

2.2. Coarse-grained molecular dynamics simulation

All MD simulations were performed using GROMACS version 5.1.4 [65]. The MARTINI force field (FF) [66] was used to describe the interactions between the lipids, water and ions. The CG potential parameters of Au beads were adopted from Song *et al.* [56] with Au beads assigned the MARTINI C5-type interaction site [44] (Table S2). The atomistic AuNP with a diameter of 3 nm was made with OpenMD [67] NP builder using a quantum-adapted variant of the Sutton-Chen force field [68] with a lattice constant of 0.408 nm used for gold. The final AuNP consisted of 887 atoms, and each atom was mapped 1:1 into CG beads (in contrast to the usual 4:1 mapping of MARTINI). During the simulations, the CG AuNP beads were connected by harmonic bonds as described elsewhere [46, 69].

Periodic boundary conditions (PBC) were applied in all directions. A cutoff of 1.2 nm was used for the non-bonded interactions, with the Lennard-Jones potential shifted between 0.9 and 1.2 nm, and the Coulomb potential shifted between 0 and 1.2 nm, such that both potentials were zero at the cut-off. Before equilibration, all systems were minimized using the steepest descent algorithm to remove any steric clashes among lipids, water, and ions molecules. In all MD

simulations, the equations of motion were integrated via the leapfrog algorithm using a 20 fs time step. The NPyT (constant particle number, pressure and temperature) ensemble was applied to the systems (Table S1) with 6 nm water slab to investigate the LS monolayer structural, dynamical and phase transformation mechanism at the interface. The systems (Table 1) with 21 nm water slab were simulated in the NVT (constant particle number, volume and temperature) ensemble to analyse the compressed or extended LS monolayer properties in the presence of AuNPs. For the NVT simulations, the APL values were fixed at 0.46 and 0.53 nm² to represent the compression and expansion states of the LS monolayers, respectively. The LS components (lipids with cholesterol), water with ions and AuNPs were coupled independently, to a velocity rescale thermostat at 310 K (close to the phase transition temperature of DPPC) with a relaxation time of 1 ps [70]. For the NPyT simulations (Table S1), Berendsen pressure barostat [71] and surface tension coupling were applied with compressibility 4.5×10^5 bar⁻¹ in the XY plane and 0 bar⁻¹ [72] along the Z-axis to have a constant box height. In these simulations, two different surface tension values 0 mN/m and 23 mN/m were used, corresponding to normal lung compression and expansion surface tensions, respectively [73]. All systems were equilibrated for 100 ns and simulated for 3 μs.

The program Visual Molecular Dynamics (VMD) [74] was used to render the snapshots from all simulations. Analyses of the order parameter, density profiles, pore formation, and radial distribution function (RDF) were carried out over the last 1 μs of each systems. The analysis of AuNPs aggregation was performed over full 3 μs of simulation using the GROMACS tool *gmx clustsize*. In this cluster size analysis, a cutoff of 1.2 nm was considered for all the systems with multiple NPs. The same cutoff value was used in the calculation of the RDFs, performed using the GROMACS tool *gmx rdf*. The RDF calculation was performed to compute the density of surfactant components with respect to AuNP beads within the cutoff distance.

3. Results and discussion

3.1. Lung surfactant monolayer area per lipid and phase behaviour

The APL of a monolayer system is used to monitor the phase transitions as well as the equilibration of the monolayer. The average APL of the systems simulated in the NPyT ensemble are given in Table S1. The results for the DPPC:POPG system indicate that the average value of the APL reduces to 0.470 ± 0.001 nm² (monolayer compression) from 0.572 ± 0.001 nm² (monolayer expansion) due to the change of surface tension to 0 mN/m from 23 mN/m, respectively. This change corresponds to a reduction in the surface area of ~15%, in

agreement with the results of an experimental study [12], where it is found that a similar level of reduction in the surface area occurred during the compression of LS monolayer. The surface tension has a linear relationship with the APL, and our obtained results follow this relationship. The relationship defines that the APL increases and decreases in harmony with the surface tension values during inspiration and expiration, respectively, replicating the expansion and compression of the alveolus surface. The presence of cholesterol in the monolayers results in a marked difference in the APL at both surface tensions (Table S1). The APL values of DPPC:POPG:CHOL drop to $0.458 \pm 0.001 \text{ nm}^2$ and $0.532 \pm 0.001 \text{ nm}^2$ at a surface tension of 0 and 23 mN/m, respectively. The LS monolayer in the presence of cholesterol reduces the lateral compressibility of the LS lipids and may lead the LS monolayer to form a LC phase at a high concentration of cholesterol, a finding that was previously reported [18].

In the initial setup of the DPPC:POPG:CHOL system with an APL of $\sim 0.61 \text{ nm}^2$, the monolayers exist in the LE phase (Fig. S2a). However, after equilibration at a surface tension $\sim 23 \text{ mN/m}$ and physiological temperature (310 K), the DPPC:POPG:CHOL monolayers transfer to LE+LC phase (Fig. S2b) with a reduction of APL. A further reduction in APL happens under a surface tension of $\sim 0 \text{ mN/m}$ while the LS monolayer undergoes compression and the monolayer transits to the LC phase (Fig. S2c). The lipids in the LS monolayer are more organized and ordered in the LC phase than the other two phases (Fig. S2). From these results and previous simulations [75], we can conclude that the LS monolayers are in the LC phase at surface tension $\sim 0 \text{ mN/m}$ and are in the LC+LE phase at surface tension $\sim 23 \text{ mN/m}$.

We have also simulated another two systems (DPPC:POPG and DPPC:POPG:CHOL) in the presence of a single AuNP only in the upper monolayer to observe the effect of single AuNP on the biophysical function of LS. For the effect of single AuNP, we have compared the results from the set of systems (DPPC:POPG and DPPC:POPG:CHOL) with and without AuNP. We have found that the single AuNP in one monolayer has a negligible effect on the structural properties of the LS monolayers, as shown in Fig. S3 and Table S1 in the supplementary information.

3.2. Effect of AuNP concentration on APL and surface tension

The effects of AuNPs concentrations on the LS monolayer at both APL are demonstrated in Fig. 2, for systems with AuNPs concentrations of $\sim 0.1\text{-}3.52 \text{ mol \%}$ of AuNPs/lipids at the two fixed APLs of 0.53 nm^2 (Fig. 2a-d) and 0.46 nm^2 (Fig. 2e-h).

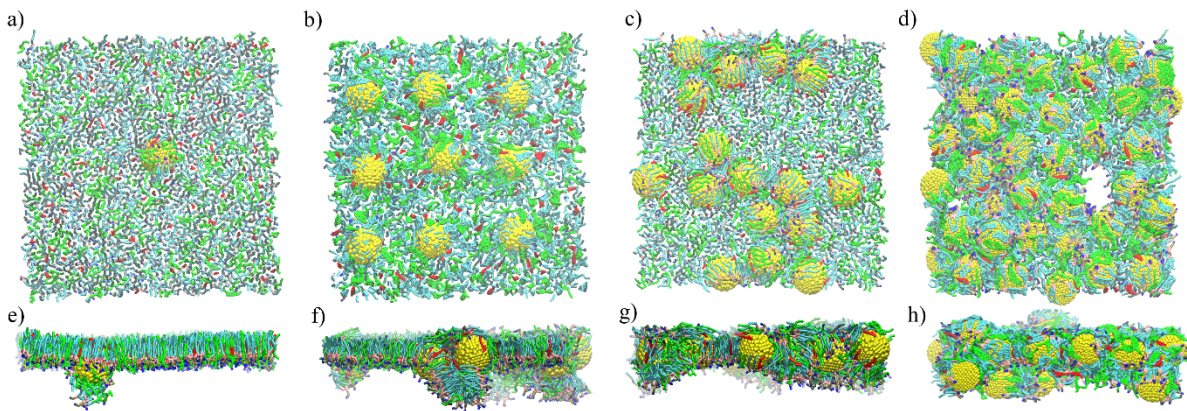


Fig. 2. Snapshots taken during the course of the simulations showing the effect of AuNPs concentrations at APL of 0.46 nm^2 (top view) (a-d), and at APL of 0.53 nm^2 (side view) (e-h) on the LS monolayers: (a and e) presenting $\sim 0.1\text{ mol \%}$ of AuNPs/lipids, (b and f) presenting $\sim 0.9\text{ mol \%}$ of AuNPs/lipids, (c and g) presenting $\sim 1.56\text{ mol \%}$ of AuNPs/lipids, and (d, h) presenting $\sim 3.52\text{ mol \%}$ of AuNPs/lipids. The surface tensions of the monolayers consisting AuNPs with the concentrations of ~ 0.1 , ~ 0.9 , ~ 1.56 , and $\sim 3.52\text{ mol \%}$ of AuNPs/lipids at APLs of 0.47 nm^2 are ~ 1.6 , ~ 25.2 , ~ 40.3 , and $\sim 41.8\text{ mN/m}$, respectively, whereas at APL of 0.53 nm^2 are ~ 21.3 , ~ 25.3 , ~ 41.9 , and $\sim 48.1\text{ mN/m}$, respectively.

At both APLs, the AuNPs become embedded in the monolayers, with the phospholipid and cholesterol molecules binding to the surface of the NPs. The lipid-coated AuNPs disrupt the monolayer structure causing bulges or “pockets” to form on the monolayer. However, these “pockets” of lipid-coated AuNP do not detach from the monolayer (Fig. 2) on the timescales simulated. The interaction of lipids with the AuNPs results in the extraction of lipids from the LS monolayer, which in turn leads to the creation of partial vacancies in the monolayer and results in the pore formation. No pores are formed in the LS monolayer at the concentrations $\leq 1.56\text{ mol \%}$ of AuNPs/lipids. To the best of author’s knowledge, no captive bubble experiment has been performed to monitor pore formation by high concentrations of AuNPs, inhibiting a direct comparison of our result against experiment. However, previous MD simulations (e.g. [7, 57]), have reported that a high concentration of spherical NPs in the monolayer leads to pore formation. In our simulations, pores are observed in the monolayers, at both the APLs simulated, at a concentration of $\sim 3.52\text{ mol \%}$ of AuNPs/lipids (see Fig. 2d and Fig. S4). The results suggest that the damage in LS monolayer strongly depends on the concentration of AuNPs and also relates to the aggregation of AuNPs, similar findings have been reported for other spherical hydrophobic NPs (e.g. [7, 57]).

LS phase behaviour and APL values are regulated by the surface tension at the air-water interface. In the healthy human body, the surface tension value remains in the range \sim 20-25 mN/m, called equilibrium surface tension, during lung alveolus expansion. During compression of the surface area upon exhalation, the surface tension value typically reduces \sim 0 mN/m. To analyse the effects of AuNPs concentration on normal surface tension values, we have performed a series of simulations in the canonical ensemble at the two APL values corresponding to surface tensions of 0 and 23 mN/m for the monolayer in the absence of AuNPs (Table 1). In the NVT simulations, high concentrations of AuNPs interfere with lowering the surface tension values of LS monolayer. It is found that a very low concentration of AuNPs (<0.1 mol % of AuNPs/lipids) does not significantly affect the properties of the LS monolayer. The evidence to this claim can be the failure of pore formation in the LS monolayers (Fig. 2a and e), most importantly the lack of change to surface tension values for single AuNP in monolayers (Fig. 3), and the minor change in lipid order parameter (Fig. 4) values. In the experimental view, bare AuNPs (as pollutants) at \sim 3.7 mol % of AuNPs/lipids concentrations interfered with the phospholipid adsorption process to form LS monolayer at the equilibrium surface tension (\sim 23 mN/m), which would disrupt natural lung function by inhibiting the lowering of the surface tension during compression process [12]. The most recent experimental studies (*in vitro*) also claim that at low concentration of AuNPs had less influence on lungs function while the higher concentrations greatly impeded the various lung properties [13]. In addition to the experimental findings, computational studies have also reported that spherical hydrophobic NPs could inhibit the LS ability to reduce the surface tension at higher concentration [7].

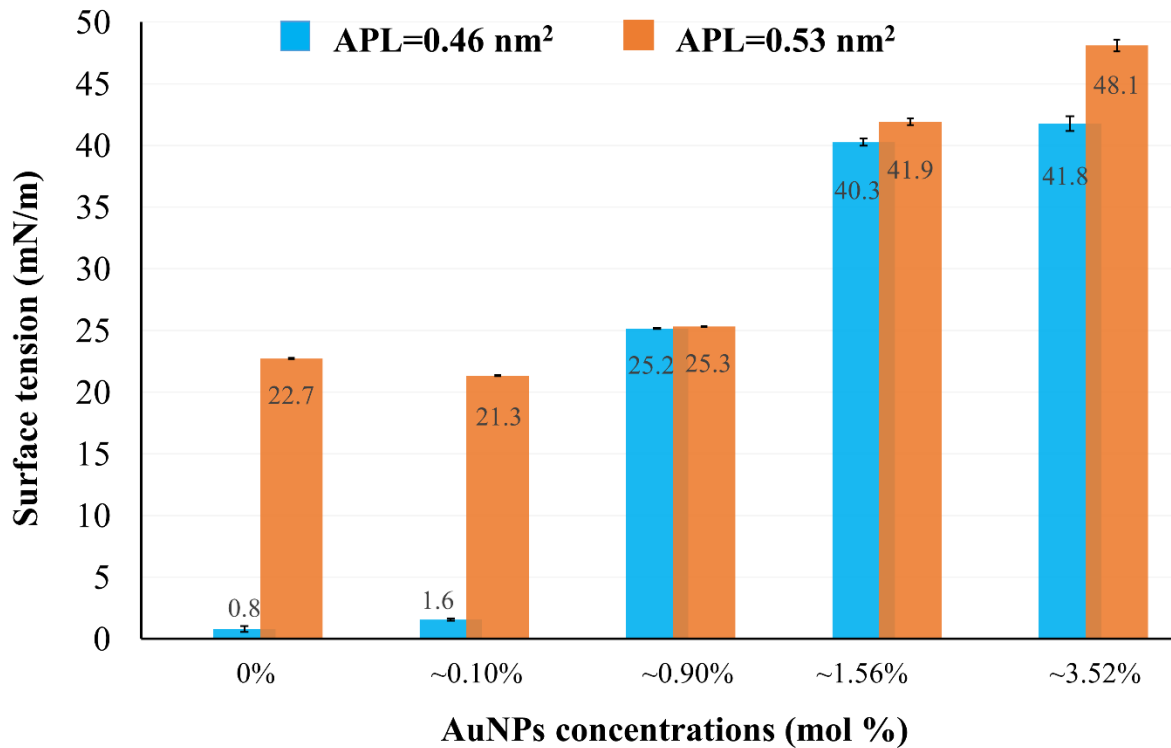


Fig. 3. Effect of AuNPs concentrations on the surface tensions for systems with fixed APL values 0.46 nm^2 , and 0.53 nm^2 . Error bars represent the error estimates using block averaging.

In the absence of NPs, LS monolayers spontaneously attain surface tensions of ~ 0 and $\sim 23 \text{ mN/m}$ by LS compression and expansion, respectively. The very low concentration ($\sim 0.1 \text{ mol \%}$ of AuNPs/lipids) of AuNPs barely affects this dynamical process (Fig. 3) of surfactant monolayers. Our simulation results indicate significant changes in the predicted value of the surface tension, resulting from the presence of AuNPs at concentrations $\geq 0.9 \text{ mol \%}$ (AuNPs/lipids), which could result in impediment of the normal function of the lungs (Fig. 3). In summary, these results show that the lower concentration of AuNPs, $\sim 0.1 \text{ mol \%}$, barely affects normal lung function whereas higher concentrations of bare AuNPs hinder lowering of the surface tension values at both surface areas, which aligns with experimental studies [12, 13].

3.3. Surfactant lipid order

Lipid order parameter calculation (supplementary information) measures the structural ordering of the lipids within a membrane. A lowering in the value of the order parameter accompanies the transformation of lipid-ordered phase to the lipid-disordered phase. The average order parameter can vary between -0.5 and 1, with -0.5 indicating perfect anti-

alignment of the lipid tails, and 1 indicating that the lipids tails are in perfect alignment). The order parameter of DPPC tail chain1 (*sn*-1) beads and POPC tail chain 2 (*sn*-2) beads at surface tension 0 mN/m and 20 mN/m are reported in Fig. S5, the obtained values are in agreement with the values published by Estrada-López *et al.* [37]. It has been noticed that saturated lipids (single bond in each chain) are more ordered, occupying less area than unsaturated (double bond in the chain) lipids like POPC and POPG.

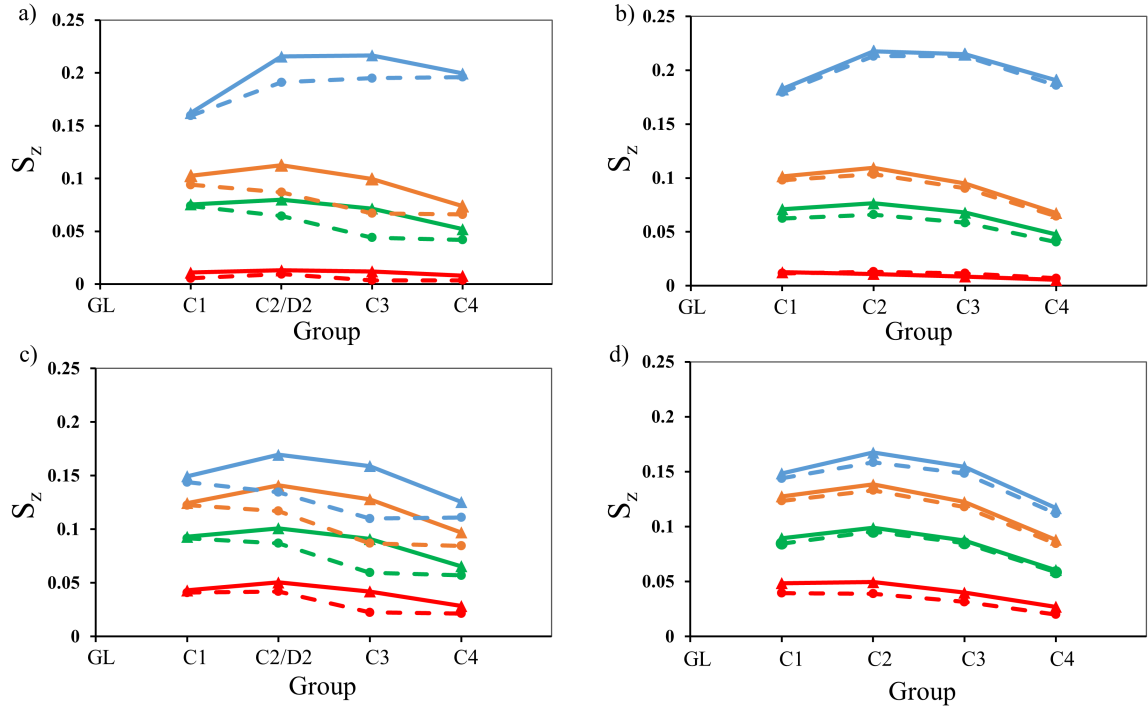


Fig. 4. AuNPs concentration (~0.1, ~0.9, ~1.56 and ~3.52 mol % of AuNPs/lipids) effects on DPPC (solid lines with triangular symbols) and POPG (dashed lines with circular symbols) lipid tails chain order parameters, chain 1 (*sn*-1) in (a, c), and chain 2 (*sn*-2) in (b, d) at APLs of 0.46 nm^2 (a, b), and 0.53 nm^2 (c, d). The ~0.1, ~0.9, ~1.56 and ~3.52 mol % concentrations of AuNPs/lipids are shown by the blue, orange, green, and red lines respectively. The surface tensions of the monolayers consisting AuNPs with the concentrations of ~0.1, ~0.9, ~1.56, and ~3.52 mol% of AuNPs/lipids at APLs of 0.47 nm^2 are ~1.6, ~25.2, ~40.3, and ~41.8 mN/m, respectively, whereas at APL of 0.53 nm^2 are ~21.3, ~25.3, ~41.9, and ~48.1 mN/m, respectively.

The average order parameters for the monolayers of DPPC:POPG and DPPC:POPG:CHOL systems are calculated at two different surface tensions in the absence (solid line) and in the presence (dashed line) of single AuNP in the upper layer (Fig. S3). Monolayer lipids start disordering at the time of the NP entering into the monolayer (Fig. S6). Visual analysis of the monolayers (Fig. S6a) shows that the lipids within ~1 nm of the NP are more disordered than those in bulk. The AuNP is partially embedded within the monolayer by 2 ns of simulation

time (Fig. S6b). After 16 ns, the AuNP starts to disturb the lipid tails at the vacuum interface and moves further towards the lipid head groups at the water interface (Fig. S6c). The presence of an AuNP in the monolayer induces buckling upon a lateral compression of the monolayer (Fig. S6b-d). This behaviour is consistent with the start of the process of monolayer collapse observed in previous studies. In the present study, the buckle in the monolayer is observed near the AuNP in one monolayer and thus failed to affect the average order parameter values of the lipids in both monolayers. On the other hand, significant differences are observed in the order parameters for the two different surface tensions (Fig. S3), with the lipids tail beads being more ordered at the lower surface tension. The presence of the double bond in the POPG *sn*-1 lipid chain makes it more disordered compared to DPPC at both surface tensions (Fig. S3). Similar to the systems with single AuNP, the presence of cholesterol also does not induce a significant change in lipid order parameter values (Fig. S3c and d). Overall, the results from simulations in the NP γ T ensemble indicate that both DPPC and POPG lipids are more disordered at higher surface tension (Fig. S3).

For the simulations performed in the canonical ensemble, the degree of lipid tail disordering in the monolayer rises along with the increase of AuNP concentration (Fig. 4). The LS monolayers lipids were found to be more disordered in the presence of AuNPs at both APLs as compared to the system in the absence of AuNPs. At the APL of 0.46 nm^2 , a sudden fall in order parameter values is observed in both chains beads of DPPC and POPG lipids for the AuNPs concentrations of ~ 0.1 to $\sim 0.9\text{ mol } \%$ and ~ 1.56 to $\sim 3.52\text{ mol } \%$ of AuNPs/lipids (Fig. 4a and b). Whereas, a gradual decrease in order parameter values is observed for ~ 0.9 to $\sim 1.56\text{ mol } \%$ of AuNPs/lipids concentrations (Fig. 4a and b) at APL of 0.46 nm^2 . The ordering of the lipid tails is moderately decreased for all concentrations of AuNPs at the APL of 0.53 nm^2 , Fig. 4c and d.

3.4. Surfactant components density

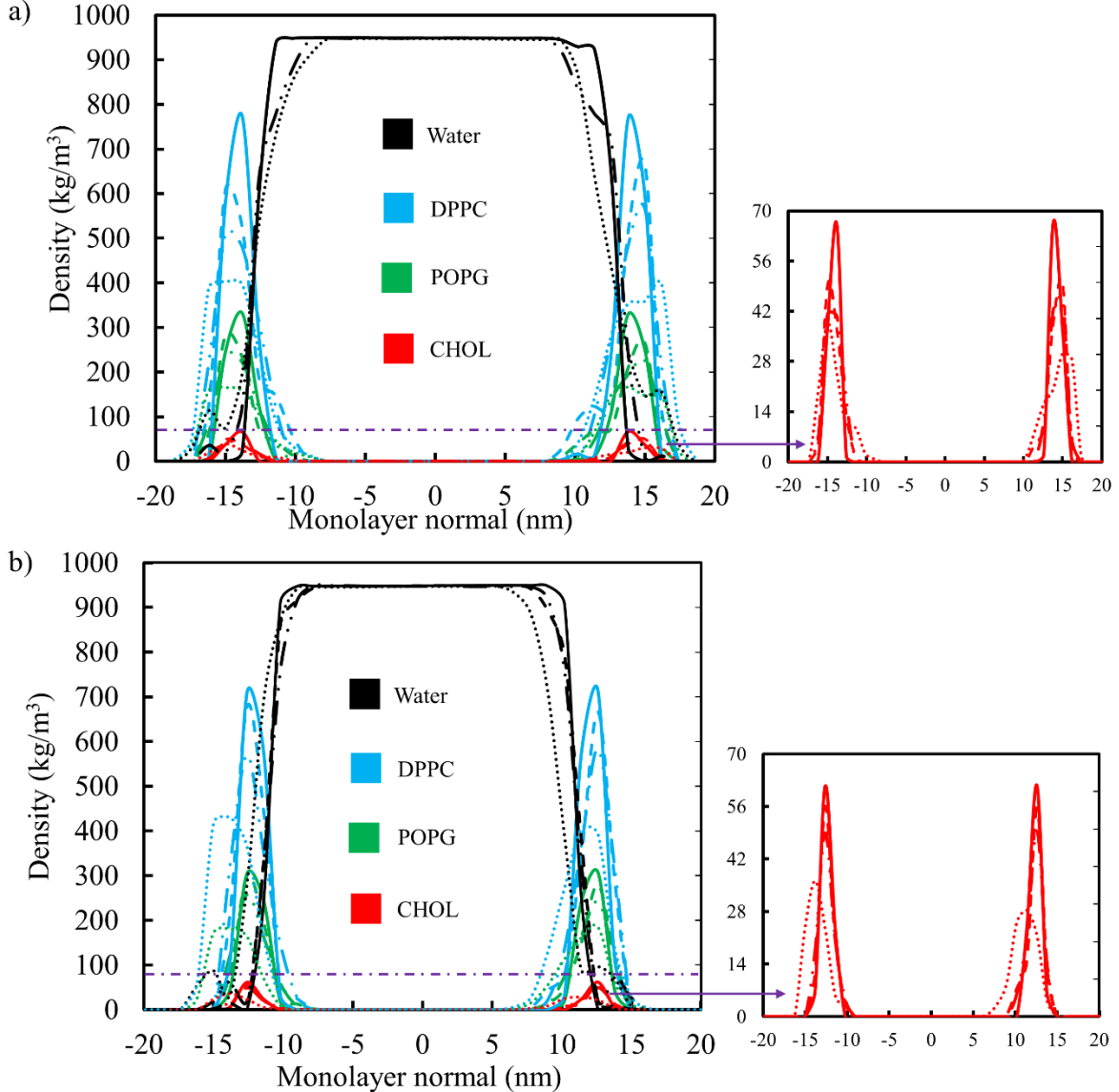


Fig. 5. AuNPs concentrations (~ 0.1 , ~ 0.9 , ~ 1.56 and ~ 3.52 mol % of AuNPs/lipids) effect on surfactant monolayer lipids, cholesterol (inset figures), and water density profiles at APLs of (a) 0.46 nm^2 , and (b) 0.53 nm^2 . Solid line represents ~ 0.1 mol % of AuNPs/lipids, dash line represents ~ 0.9 mol % AuNPs/lipids, dash-dotted line represents ~ 1.56 mol % of AuNPs/lipids, and dotted line represents ~ 3.52 mol % of AuNPs/lipids concentrations. The surface tensions of the monolayers consisting AuNPs with the concentrations of ~ 0.1 , ~ 0.9 , ~ 1.56 , and ~ 3.52 mol% of AuNPs/lipids at APLs of 0.47 nm^2 are ~ 1.6 , ~ 25.2 , ~ 40.3 , and $\sim 41.8 \text{ mN/m}$, whereas at APL of 0.53 nm^2 are ~ 21.3 , ~ 25.3 , ~ 41.9 , and $\sim 48.1 \text{ mN/m}$, respectively.

The density profiles of the LS components have been calculated at all the concentrations of AuNPs (~ 0.1 , ~ 0.9 , ~ 1.56 and ~ 3.52 mol % of AuNPs/lipids) used in our study (Fig. 5). The peaks in the density profiles of the lipids at the vacuum-water interface are higher for the system with an APL of 0.46 nm^2 (Fig. 5a) than the system with an APL of 0.53 nm^2 (Fig. 5b) indicating the more densely packed nature of the monolayer lipids at the lower surface area. The presence

of AuNPs at concentrations >0.9 mol % of AuNPs/lipids significantly affect lipids average density profiles. The height of the peaks in the density profiles of the lipids drops with the increase in AuNP concentration (Fig. 5a and b). The tendency continues when the concentrations of AuNPs increases from ~0.9 to ~1.52 mol % and from ~1.52 to ~3.52 mol %. Similar to the effects of AuNPs concentrations on other LS lipids, the height of the peaks in the cholesterol density profiles (see Figure 5 insets) decrease with the increase of AuNPs concentrations.

3.5. AuNP aggregation in LS monolayer

The aggregation of the AuNPs in LS monolayer over time was studied using a cluster size analysis. A cutoff of 1.2 nm is considered, meaning that two AuNPs are considered to be aggregated in one cluster when they were less than 1.2 nm apart from each other.

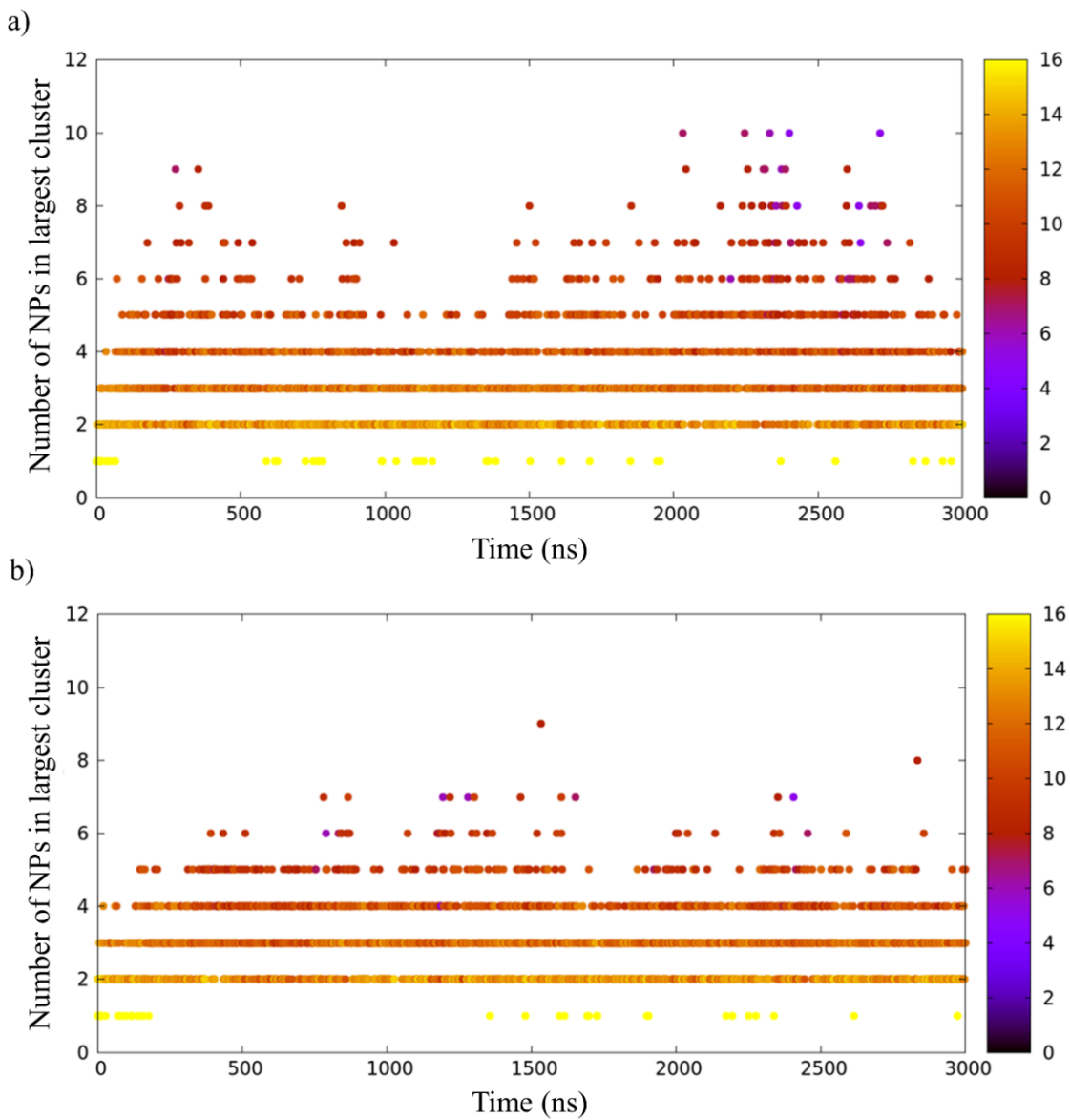


Fig. 6. Cluster size analysis of AuNPs (~ 1.56 mol % of AuNPs/lipids) at APLs of (a) 0.46 nm^2 , and (b) 0.53 nm^2 . Simulation time is presented along the X-axis, the number of AuNPs in the largest cluster is presented along the Y-axis, and the number of clusters is indicated by different colours. The surface tensions of the monolayers at APLs of 0.47 and 0.53 nm^2 are ~ 40.3 and $\sim 41.9\text{ mN/m}$, respectively.

The cluster size analyses of AuNPs at the concentrations of ≥ 0.9 mol % of AuNPs/lipids are plotted for the systems with APL of 0.46 nm^2 (Fig. 6a, Fig. S7a and Fig. S8a) and APL of 0.53 nm^2 (Fig. 6b, Fig. S7b and Fig. S8b). At the beginning of the simulations, the system with ~ 1.56 mol % of AuNPs/lipids concentration contains 16 AuNPs in each monolayer, with all AuNPs separated by more than cutoff distance, resulting in 16 clusters (Fig. 6). As the simulation progresses, the AuNPs become embedded in the monolayer, where they aggregate as clusters of multiple AuNPs. This implies that AuNPs first interact with lipids and cholesterol in the monolayer before aggregation. The AuNPs aggregation in LS monolayer is affected by

the monolayer interfacial surface tension and the AuNP concentration (*vide infra*) [7, 27]. Also, many other factors such as chemical composition, potential, size, shape and hydrophobicity influence NP aggregation [60]. In our study, we have observed that once the AuNPs become embedded in the monolayer, they quickly become coated with lipids and then proceed to aggregate together. The extent to which, and how, lipids mediate this aggregation is a challenging question and will be the subject of future studies. However, there is some evidence from previous studies that a reverse micellar structure forming around NPs may play a role in NP aggregation [57].

The number of clusters and the number of AuNPs in the largest cluster fluctuate over time. More clusters are formed at the lower APL (Fig. 6a, Fig. S7a and Fig. S8a) than the higher APL (Fig. 6b, Fig. S7b and Fig. S8b). Also, the chance of forming a cluster depends on the number of NPs in the system. It is very usual that the high concentration of AuNPs has more possibility of aggregating together to form clusters than the low concentration. In support of this claim, we have presented the cluster analysis for the concentration of ~3.52 mol % of AuNPs/lipids at APL of 0.46 nm^2 (Fig. S7a) and 0.53 nm^2 (Fig. S7b). At this concentration, 36 AuNPs are in each LS monolayer at the beginning of the simulations, and the distance between two AuNPs is less than the cutoff value. As a result, all 36 AuNPs are in a single cluster, and the number of NPs in the largest cluster is reduced with the increase of simulation time. Cluster size analysis is also performed over ~0.9 mol % of AuNPs/lipids system at both APL values (Fig. S8). From Figs. 6, S7 and S8, it is clear that the number of NPs in a cluster increases with the increase of AuNPs concentration. At ~0.9 mol % of AuNPs/lipids, the largest cluster contains only 3 AuNPs (Fig. S8b) while this number has increased to 9 (Fig. 6b) and 24 (Fig. S7b) at the concentrations of ~1.56 mol % and ~3.52 mol % of AuNPs/lipids, respectively at the APL of 0.53 nm^2 . At the lower surface area, the AuNPs aggregate more quickly. Therefore, the possibility of forming a larger size cluster has also increased.

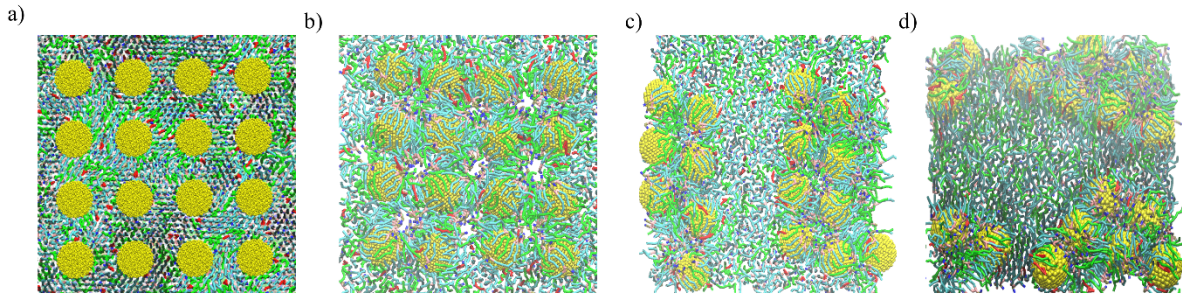


Fig. 7. (a) AuNPs cluster formation over time at the APL of 0.46 nm^2 . The concentration was $\sim 1.56 \text{ mol \%}$ of AuNPs/lipids. The representative snapshots (top view) are taken at (a) 0, (b) 10, (c) 500, and (d) 3000 ns. The surface tension of the monolayer is $\sim 40.3 \text{ mN/m}$ for last $1 \mu\text{s}$ simulation.

The process of AuNPs aggregation in the LS monolayer is illustrated in Fig. 7, where the formation of AuNP clusters is tracked through the simulation (0, 10, 500, and 3000 ns) for an exemplary system ($\sim 1.56 \text{ mol \%}$ of AuNPs/lipids at $\text{APL}=0.46 \text{ nm}^2$). The snapshots indicate the AuNPs aggregation in the surfactant monolayer started when the AuNPs absorbed in the monolayer (Fig. 7). In the initial setup, the 16 AuNPs are separated by about 3 nm distance from each other (Fig. 7a) and are placed $\sim 1 \text{ nm}$ above the monolayer. With increasing simulation time ($t=10 \text{ ns}$) the NPs become fully submerged in the monolayer (Fig. 7b), wrapped by phospholipids and cholesterol molecules. As the simulation progresses (500 ns to 3000 ns), more lipids and cholesterol adsorb to the NPs surface, and the NPs begin to aggregate, forming clusters of different sizes (Fig. 7c and d).

3.6. Radial distribution function

The RDF of each lipid and cholesterol with the beads in the AuNP are illustrated in Fig. 8a for both APL (0.46 and 0.56 nm^2), at a concentration of $\sim 0.1 \text{ mol \%}$ of AuNPs/lipids.

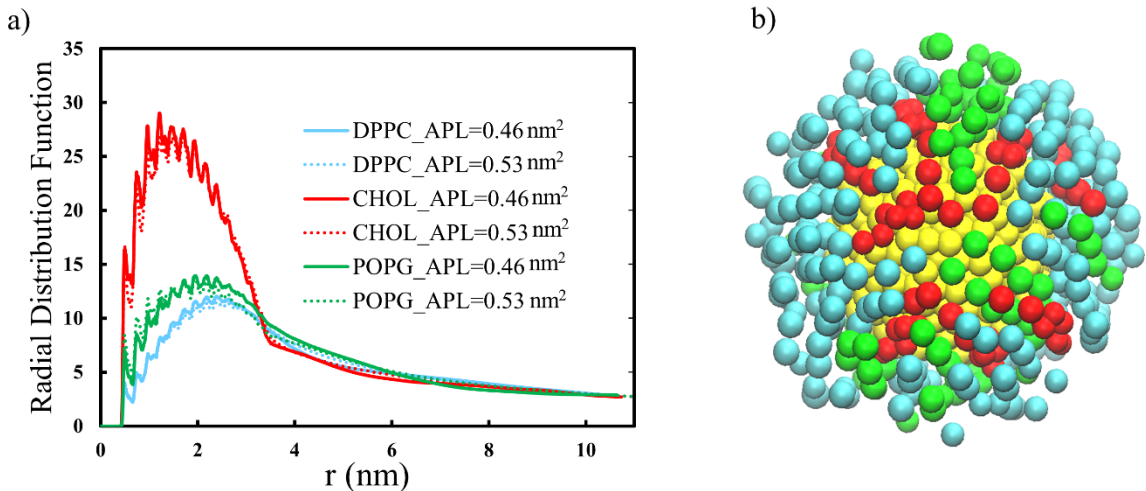


Fig. 8. The radial distribution function (RDF) between Au beads and lipid monolayer components at APLs of 0.46 nm^2 (solid line), and 0.53 nm^2 (dot) (b) snapshot of the interaction of AuNP (yellow) beads with DPPC (cyan), POPG (green) and cholesterol (red) beads within a cutoff distance 1.2 nm during lung compression. The surface tensions of the monolayers at APLs of 0.47 and 0.53 nm^2 are ~ 1.6 and $\sim 21.3\text{ mN/m}$, respectively.

The distribution of lipid and cholesterol beads in the vicinity of an AuNP is shown in Fig. 8b. There is a clear preference for the adsorption of cholesterol to the AuNP over other two surfactant lipids (DPPC and POPG). This preference is probably driven by the fact that cholesterol is both more hydrophobic and more rigid than the other two lipids. The preferential binding of cholesterol to AuNPs could affect the long-range structure of LS monolayers by disturbing the distribution of cholesterol within the monolayers.

4. Conclusions

In this work, the effect of bare AuNPs on a simplified model of a LS monolayer consisting of lipids and cholesterol has been studied using coarse-grained molecular dynamics simulation. AuNP concentrations of $\sim 0.1\text{-}3.52\text{ mol \%}$ have been investigated at two different surface areas/APL. It has been found that the AuNPs may disrupt the normal biophysical activity of lungs under high concentration of AuNPs, resulting in higher surface tension at the vacuum-water interface. The obtained results also indicate that AuNPs concentration plays a significant role in the order parameters of lipid tail beads. The interactions between AuNPs and lipids induce a decrease in order parameter values and density profiles of LS components. The further reduction in the order parameter and peaks in the density profiles are observed when the concentration of AuNPs increases. The AuNPs cluster size in LS monolayer increases with

AuNP concentration and decreases as the surface area of the LS monolayer increases. At an AuNP concentration of ~3.52 mol %, pores form in the LS monolayers with APLs of 0.46 and 0.53 nm². Cholesterol molecules and the hydrophobic tails of the amphiphilic lipids interact with AuNPs, with cholesterol preferentially adsorbing to the surface of the AuNP over the phospholipid tails. The consequence of this disruption of the LS monolayer is that the normal functions of the lungs are affected. More specifically, AuNPs hinder the ability of the LS monolayer to achieve normal surface tension during breathing. Overall, the study provides molecular insights of model AuNPs (as pollutants) with model LS monolayer at the vacuum-water interface. The findings of this study bring to light the possible consequences of AuNP inhalation and the possible causes of those effects. The results of this study provide clear and understandable molecular insights that could be helpful to design future nanomedicine along with the assessment of AuNP as a pollutant. Also, the results of our model simulations will assist in understanding different lung diseases due to the inhalation of environmental NPs in different concentration levels. Furthermore, the study will help to identify the potential health risk in people dealing with bare AuNP as an engineered nanoparticle in the laboratory or gold mines.

Authors' contributions

S.I.H developed model, performed simulations, analysed data and drafted the manuscript. S.C.S coordinated the study, N.S.G conceived the study, Z.E.H helped in concept clarification, and Y.T.G. provided comments on the manuscript. S.C.S, N.S.G, Z.E.H and Y.T.G. helped draft the manuscript. All authors gave their final permission for publication.

Competing interest

The authors have no conflict of interests to disclose.

Funding

This work was completed with the support of University of Technology Sydney (UTS) FEIT Research Scholarship, UTS IRS (S.I.H.), 2018 Blue Sky scheme–Suvash Saha (Activity 2232368), N.S.G is supported by the Vice-Chancellor fellowship funded by QUT. The computational facilities were provided by the UTS eResearch High-Performance Computer Cluster, QUT HPC and NCI Australia.

Supplementary data

Supplementary data (the AuNP itp, topology, and gro files) associated with this article will be available upon request (suvash.saha@uts.edu.au).

References:

- [1] Yeh, Y.-C., Creran, B. & Rotello, V.M. 2012 Gold nanoparticles: preparation, properties, and applications in bionanotechnology. *Nanoscale* **4**, 1871-1880. (doi:10.1039/C1NR11188D).
- [2] Lin, X., Bai, T., Zuo, Y.Y. & Gu, N. 2014 Promote potential applications of nanoparticles as respiratory drug carrier: insights from molecular dynamics simulations. *Nanoscale* **6**, 2759-2767. (doi:10.1039/c3nr04163h).
- [3] Rossi, G. & Monticelli, L. 2016 Gold nanoparticles in model biological membranes: A computational perspective. *Biochimica et Biophysica Acta (BBA) - Biomembranes* **1858**, 2380-2389. (doi:10.1016/j.bbamem.2016.04.001).
- [4] Dreaden, E.C., Alkilany, A.M., Huang, X., Murphy, C.J. & El-Sayed, M.A. 2012 The golden age: gold nanoparticles for biomedicine. *Chemical Society Reviews* **41**, 2740-2779. (doi:10.1039/C1CS15237H).
- [5] Valle, R.P., Wu, T. & Zuo, Y.Y. 2015 Biophysical Influence of Airborne Carbon Nanomaterials on Natural Pulmonary Surfactant. *ACS Nano* **9**, 5413-5421. (doi:10.1021/acsnano.5b01181).
- [6] Barnoud, J., Urbini, L. & Monticelli, L. 2015 C60 fullerene promotes lung monolayer collapse. *Journal of The Royal Society Interface* **12**. (doi:10.1098/rsif.2014.0931).
- [7] Nisoh, N., Karttunen, M., Monticelli, L. & Wong-ekkabut, J. 2015 Lipid monolayer disruption caused by aggregated carbon nanoparticles. *RSC Advances* **5**, 11676-11685. (doi:10.1039/C4RA17006G).
- [8] Li, N., Hao, M., Phalen, R.F., Hinds, W.C. & Nel, A.E. 2003 Particulate air pollutants and asthma. A paradigm for the role of oxidative stress in PM-induced adverse health effects. *Clinical immunology (Orlando, Fla.)* **109**, 250-265.
- [9] Pope, I.C., Burnett, R.T., Thun, M.J. & et al. 2002 Lung cancer, cardiopulmonary mortality, and long-term exposure to fine particulate air pollution. *The Journal of the American Medical Association* **287**, 1132-1141. (doi:10.1001/jama.287.9.1132).
- [10] Xu, Y., Luo, Z., Li, S., Li, W., Zhang, X., Zuo, Y.Y., Huang, F. & Yue, T. 2017 Perturbation of the pulmonary surfactant monolayer by single-walled carbon nanotubes: a molecular dynamics study. *Nanoscale* **9**, 10193-10204. (doi:10.1039/C7NR00890B).
- [11] Yue, T., Xu, Y., Li, S., Luo, Z., Zhang, X. & Huang, F. 2017 Surface patterning of single-walled carbon nanotubes enhances their perturbation on a pulmonary surfactant monolayer: frustrated translocation and bilayer vesiculation. *RSC Advances* **7**, 20851-20864. (doi:10.1039/C7RA01392B).
- [12] Bakshi, M.S., Zhao, L., Smith, R., Possmayer, F. & Petersen, N.O. 2008 Metal Nanoparticle Pollutants Interfere with Pulmonary Surfactant Function In Vitro. *Biophysical Journal* **94**, 855-868. (doi:10.1529/biophysj.107.106971).
- [13] Zhang, K., Liu, L., Bai, T. & Guo, Z. 2018 Interaction Between Hydrophobic Au Nanoparticles and Pulmonary Surfactant (DPPC) Monolayers. *Journal of biomedical nanotechnology* **14**, 526-535. (doi:10.1166/jbn.2018.2497).
- [14] Luo, Z., Li, S., Xu, Y., Yan, Z., Huang, F. & Yue, T. 2018 The role of nanoparticle shape in translocation across the pulmonary surfactant layer revealed by molecular dynamics simulations. *Environmental Science: Nano* **5**, 1921-1932. (doi:10.1039/C8EN00521D).

- [15] Parra, E. & Pérez-Gil, J. 2015 Composition, structure and mechanical properties define performance of pulmonary surfactant membranes and films. *Chemistry and Physics of Lipids* **185**, 153-175. (doi:10.1016/j.chemphyslip.2014.09.002).
- [16] Veldhuizen, R., Nag, K., Orgeig, S. & Possmayer, F. 1998 The role of lipids in pulmonary surfactant. *Biochimica et Biophysica Acta (BBA) - Molecular Basis of Disease* **1408**, 90-108. (doi:10.1016/S0925-4439(98)00061-1).
- [17] Zhang, H., Wang, Y.E., Fan, Q. & Zuo, Y.Y. 2011 On the Low Surface Tension of Lung Surfactant. *Langmuir* **27**, 8351-8358. (doi:10.1021/la201482n).
- [18] Laing, C., Baoukina, S. & Peter Tielemans, D. 2009 Molecular dynamics study of the effect of cholesterol on the properties of lipid monolayers at low surface tensions. *Physical Chemistry Chemical Physics* **11**, 1916-1922. (doi:10.1039/B819767A).
- [19] Veldhuizen, E.J.A. & Haagsman, H.P. 2000 Role of pulmonary surfactant components in surface film formation and dynamics. *Biochimica et Biophysica Acta (BBA) - Biomembranes* **1467**, 255-270. (doi:10.1016/S0005-2736(00)00256-X).
- [20] Baoukina, S., Monticelli, L., Risselada, H.J., Marrink, S.J. & Tielemans, D.P. 2008 The molecular mechanism of lipid monolayer collapse. *Proceedings of the National Academy of Sciences of the United States of America* **105**, 10803-10808. (doi:10.1073/pnas.0711563105).
- [21] Duncan, S.L., Dalal, I.S. & Larson, R.G. 2011 Molecular dynamics simulation of phase transitions in model lung surfactant monolayers. *Biochimica et Biophysica Acta (BBA) - Biomembranes* **1808**, 2450-2465. (doi:10.1016/j.bbamem.2011.06.026).
- [22] Ortiz-Collazos, S., Estrada-Lopez, E.D., Pedreira, A.A., Picciani, P.H.S., Oliveira, O.N., Jr. & Pimentel, A.S. 2017 Interaction of levofloxacin with lung surfactant at the air-water interface. *Colloids and surfaces. B, Biointerfaces* **158**, 689-696. (doi:10.1016/j.colsurfb.2017.07.066).
- [23] Baoukina, S., Mendez-Villuendas, E. & Tielemans, D.P. 2012 Molecular View of Phase Coexistence in Lipid Monolayers. *Journal of the American Chemical Society* **134**, 17543-17553. (doi:10.1021/ja304792p).
- [24] Schürch, S., Green, F.H.Y. & Bachofen, H. 1998 Formation and structure of surface films: captive bubble surfactometry. *Biochimica et Biophysica Acta (BBA) - Molecular Basis of Disease* **1408**, 180-202. (doi:10.1016/S0925-4439(98)00067-2).
- [25] Baoukina, S. & Tielemans, D.P. 2016 Computer simulations of lung surfactant. *Biochimica et Biophysica Acta (BBA) - Biomembranes* **1858**, 2431-2440. (doi:10.1016/j.bbamem.2016.02.030).
- [26] Yue, T., Xu, Y., Li, S., Luo, Z., Zhang, X. & Huang, F. 2017 Ultrashort Single-Walled Carbon Nanotubes Insert into a Pulmonary Surfactant Monolayer via Self-Rotation: Poration and Mechanical Inhibition. *The Journal of Physical Chemistry B* **121**, 2797-2807. (doi:10.1021/acs.jpcb.7b00297).
- [27] Chiu, C.-c., Shinoda, W., DeVane, R.H. & Nielsen, S.O. 2012 Effects of spherical fullerene nanoparticles on a dipalmitoyl phosphatidylcholine lipid monolayer: a coarse grain molecular dynamics approach. *Soft Matter* **8**, 9610-9616. (doi:10.1039/C2SM26357B).
- [28] Luo, Z., Li, S., Xu, Y., Ren, H., Zhang, X., Hu, G., Huang, F. & Yue, T. 2018 Extracting pulmonary surfactants to form inverse micelles on suspended graphene nanosheets. *Environmental Science: Nano* **5**, 130-140. (doi:10.1039/C7EN00843K).
- [29] Hu, Q., Jiao, B., Shi, X., Valle, R.P., Zuo, Y.Y. & Hu, G. 2015 Effects of graphene oxide nanosheets on the ultrastructure and biophysical properties of the pulmonary surfactant film. *Nanoscale* **7**, 18025-18029. (doi:10.1039/c5nr05401j).
- [30] Yue, T., Wang, X., Zhang, X. & Huang, F. 2015 Molecular modeling of interaction between lipid monolayer and graphene nanosheets: implications for pulmonary

- nanotoxicity and pulmonary drug delivery. *RSC Advances* **5**, 30092-30106. (doi:10.1039/C5RA04922A).
- [31] Katiyar, P. & Singh, J.K. 2017 A coarse-grain molecular dynamics study of oil-water interfaces in the presence of silica nanoparticles and nonionic surfactants. *The Journal of Chemical Physics* **146**, 204702. (doi:10.1063/1.4984073).
- [32] Lin, X., Zuo, Y.Y. & Gu, N. 2015 Shape affects the interactions of nanoparticles with pulmonary surfactant. *Science China Materials* **58**, 28-37. (doi:10.1007/s40843-014-0018-5).
- [33] Hu, G., Jiao, B., Shi, X., Valle, R.P., Fan, Q. & Zuo, Y.Y. 2013 Physicochemical Properties of Nanoparticles Regulate Translocation across Pulmonary Surfactant Monolayer and Formation of Lipoprotein Corona. *ACS Nano* **7**, 10525-10533. (doi:10.1021/nn4054683).
- [34] Bai, X., Xu, M., Liu, S. & Hu, G. 2018 Computational Investigations of the Interaction between the Cell Membrane and Nanoparticles Coated with a Pulmonary Surfactant. *ACS Applied Materials & Interfaces* **10**, 20368-20376. (doi:10.1021/acsami.8b06764).
- [35] Stachowicz-Kusnierz, A., Trojan, S., Cwiklik, L., Korchowiec, B. & Korchowiec, J. 2017 Modeling Lung Surfactant Interactions with Benzo[a]pyrene. *Chemistry (Weinheim an der Bergstrasse, Germany)* **23**, 5307-5316. (doi:10.1002/chem.201605945).
- [36] Souza, L.M.P., Nascimento, J.B., Romeu, A.L., Estrada-López, E.D. & Pimentel, A.S. 2018 Penetration of antimicrobial peptides in a lung surfactant model. *Colloids and Surfaces B: Biointerfaces* **167**, 345-353. (doi:10.1016/j.colsurfb.2018.04.030).
- [37] Estrada-Lopez, E.D., Murce, E., Franca, M.P.P. & Pimentel, A.S. 2017 Prednisolone adsorption on lung surfactant models: insights on the formation of nanoaggregates, monolayer collapse and prednisolone spreading. *RSC Advances* **7**, 5272-5281. (doi:10.1039/C6RA28422A).
- [38] Xu, Y., Deng, L., Ren, H., Zhang, X., Huang, F. & Yue, T. 2017 Transport of nanoparticles across pulmonary surfactant monolayer: a molecular dynamics study. *Physical Chemistry Chemical Physics* **19**, 17568-17576. (doi:10.1039/C7CP02548C).
- [39] Chen, P., Zhang, Z., Gu, N. & Ji, M. 2018 Effect of the surface charge density of nanoparticles on their translocation across pulmonary surfactant monolayer: a molecular dynamics simulation. *Molecular Simulation* **44**, 85-93. (doi:10.1080/08927022.2017.1342118).
- [40] Hu, Q., Bai, X., Hu, G. & Zuo, Y.Y. 2017 Unveiling the Molecular Structure of Pulmonary Surfactant Corona on Nanoparticles. *ACS Nano* **11**, 6832-6842. (doi:10.1021/acsnano.7b01873).
- [41] Porta, F., Speranza, G., Krpetić, Ž., Dal Santo, V., Francescato, P. & Scarì, G. 2007 Gold nanoparticles capped by peptides. *Materials Science and Engineering: B* **140**, 187-194. (doi:10.1016/j.mseb.2007.03.019).
- [42] Xu, Y., Li, S., Luo, Z., Ren, H., Zhang, X., Huang, F., Zuo, Y.Y. & Yue, T. 2018 Role of Lipid Coating in the Transport of Nanodroplets across the Pulmonary Surfactant Layer Revealed by Molecular Dynamics Simulations. *Langmuir* **34**, 9054-9063. (doi:10.1021/acs.langmuir.8b01547).
- [43] Ramazani, A., Mandal, T. & Larson, R.G. 2016 Modeling the Hydrophobicity of Nanoparticles and Their Interaction with Lipids and Proteins. *Langmuir* **32**, 13084-13094. (doi:10.1021/acs.langmuir.6b01963).
- [44] Lin, J., Zhang, H., Chen, Z. & Zheng, Y. 2010 Penetration of Lipid Membranes by Gold Nanoparticles: Insights into Cellular Uptake, Cytotoxicity, and Their Relationship. *ACS Nano* **4**, 5421-5429. (doi:10.1021/nn1010792).

- [45] Gupta, R. & Rai, B. 2017 Effect of Size and Surface Charge of Gold Nanoparticles on their Skin Permeability: A Molecular Dynamics Study. *Scientific Reports-Uk* **7**, 45292. (doi:10.1038/srep45292).
- [46] Lopez-Acevedo, O., Akola, J., Whetten, R.L., Grönbeck, H. & Häkkinen, H. 2009 Structure and Bonding in the Ubiquitous Icosahedral Metallic Gold Cluster Au₁₄₄(SR)60. *The Journal of Physical Chemistry C* **113**, 5035-5038. (doi:10.1021/jp8115098).
- [47] Kobayashi, K., Wei, J., Iida, R., Ijiro, K. & Niikura, K. 2014 Surface engineering of nanoparticles for therapeutic applications. *Polymer Journal* **46**, 460-468. (doi:10.1038/pj.2014.40).
- [48] Lin, J.-Q., Zhang, H.-W., Chen, Z., Zheng, Y.-G., Zhang, Z.-Q. & Ye, H.-F. 2011 Simulation Study of Aggregations of Monolayer-Protected Gold Nanoparticles in Solvents. *The Journal of Physical Chemistry C* **115**, 18991-18998. (doi:10.1021/jp204735d).
- [49] Granmayeh Rad, A., Abbasi, H. & Afzali, M.H. 2011 Gold Nanoparticles: Synthesising, Characterizing and Reviewing Novel Application in Recent Years. *Physics Procedia* **22**, 203-208. (doi:10.1016/j.phpro.2011.11.032).
- [50] Sung, J.H., Ji, J.H., Park, J.D., Song, M.Y., Song, K.S., Ryu, H.R., Yoon, J.U., Jeon, K.S., Jeong, J., Han, B.S., et al. 2011 Subchronic inhalation toxicity of gold nanoparticles. *Particle and fibre toxicology* **8**, 16-16. (doi:10.1186/1743-8977-8-16).
- [51] Wiles, F.J. & Faure, M.H. 1975 Chronic obstructive lung disease in gold miners. *Inhaled particles* **4 Pt 2**, 727-735.
- [52] Ayaaba, E., Li, Y., Yuan, J. & Ni, C. 2017 Occupational Respiratory Diseases of Miners from Two Gold Mines in Ghana. *International Journal of Environmental Research and Public Health* **14**, 337. (doi:10.3390/ijerph14030337).
- [53] Lansdown, A.B.G. 2018 GOLD: human exposure and update on toxic risks. *Critical reviews in toxicology* **48**, 596-614. (doi:10.1080/10408444.2018.1513991).
- [54] Miller, M.R., Raftis, J.B., Langrish, J.P., McLean, S.G., Samutrtai, P., Connell, S.P., Wilson, S., Vesey, A.T., Fokkens, P.H.B., Boere, A.J.F., et al. 2017 Inhaled Nanoparticles Accumulate at Sites of Vascular Disease. *ACS Nano* **11**, 4542-4552. (doi:10.1021/acsnano.6b08551).
- [55] Walker, N. NTP Research Concept: Nanoscale Gold. [https://ntp.niehs.nih.gov/ntp/noms/final_resconcept/nanoscale_gold_508.pdf], accessed on 10/01/2019.
- [56] Song, B., Yuan, H., Jameson, C.J. & Murad, S. 2011 Permeation of nanocrystals across lipid membranes. *Molecular Physics* **109**, 1511-1526. (doi:10.1080/00268976.2011.569511).
- [57] Yue, T., Xu, Y., Li, S., Zhang, X. & Huang, F. 2016 Lipid extraction mediates aggregation of carbon nanospheres in pulmonary surfactant monolayers. *Physical Chemistry Chemical Physics* **18**, 18923-18933. (doi:10.1039/c6cp01957a).
- [58] Konduru, N.V., Molina, R.M., Swami, A., Damiani, F., Pyrgiotakis, G., Lin, P., Andreozzi, P., Donaghey, T.C., Demokritou, P. & Krol, S. 2017 Protein corona: implications for nanoparticle interactions with pulmonary cells. *Particle and fibre toxicology* **14**, 42.
- [59] Limbach, L.K., Wick, P., Manser, P., Grass, R.N., Bruinink, A. & Stark, W.J. 2007 Exposure of engineered nanoparticles to human lung epithelial cells: influence of chemical composition and catalytic activity on oxidative stress. *Environmental science & technology* **41**, 4158-4163.
- [60] Oecd. 2012 Guidance on sample preparation and dosimetry for the safety testing of manufactured nanomaterials. OECD, paris. ENV/JM/MONO(2012)40 [[http://www.oecd.org/officialdocuments/publicdisplaydocumentpdf/?cote=ENV/JM/MONO\(2012\)40&docLanguage=En](http://www.oecd.org/officialdocuments/publicdisplaydocumentpdf/?cote=ENV/JM/MONO(2012)40&docLanguage=En)], accessed on 10/02/2019.

- [61] Baoukina, S., Monticelli, L., Amrein, M. & Tieleman, D.P. 2007 The Molecular Mechanism of Monolayer-Bilayer Transformations of Lung Surfactant from Molecular Dynamics Simulations. *Biophysical Journal* **93**, 3775-3782. (doi:10.1529/biophysj.107.113399).
- [62] Leonenko, Z., Gill, S., Baoukina, S., Monticelli, L., Doehner, J., Gunasekara, L., Felderer, F., Rodenstein, M., Eng, L.M. & Amrein, M. 2007 An elevated level of cholesterol impairs self-assembly of pulmonary surfactant into a functional film. *Biophysical Journal* **93**, 674-683. (doi:10.1529/biophysj.107.106310).
- [63] Wassenaar, T.A., Ingolfsson, H.I., Bockmann, R.A., Tieleman, D.P. & Marrink, S.J. 2015 Computational Lipidomics with insane: A Versatile Tool for Generating Custom Membranes for Molecular Simulations. *Journal of Chemical Theory and Computation* **11**, 2144-2155. (doi:10.1021/acs.jctc.5b00209).
- [64] Siebert, T.A. & Rugonyi, S. 2008 Influence of Liquid-Layer Thickness on Pulmonary Surfactant Spreading and Collapse. *Biophysical Journal* **95**, 4549-4559. (doi:10.1529/biophysj.107.127654).
- [65] Abraham, M.J., Murtola, T., Schulz, R., Páll, S., Smith, J.C., Hess, B. & Lindahl, E. 2015 GROMACS: High performance molecular simulations through multi-level parallelism from laptops to supercomputers. *SoftwareX* **1–2**, 19-25. (doi:10.1016/j.softx.2015.06.001).
- [66] Marrink, S.J., Risselada, H.J., Yefimov, S., Tieleman, D.P. & de Vries, A.H. 2007 The MARTINI force field: Coarse grained model for biomolecular simulations. *Journal of Physical Chemistry B* **111**, 7812-7824. (doi:10.1021/jp071097f).
- [67] Gezelter, J. D.; Kuang, S.; Marr, J.; Stocker, K.; Li, C.; Vardeman, C. F.; Lin, T.; Fennell, C. J.; Sun, X.; Daily, K.; Zheng, Y. OpenMD, an Open Source Engine for Molecular Dynamics; University of Notre Dame: Notre Dame, IN. <http://openmd.org/> (accessed April 21, 2017).
- [68] Sutton, A. & Chen, J. 1990 Long-range finnis-sinclair potentials. *Philosophical Magazine Letters* **61**, 139-146.
- [69] Salassi, S., Simonelli, F., Bochicchio, D., Ferrando, R. & Rossi, G. 2017 Au Nanoparticles in Lipid Bilayers: A Comparison between Atomistic and Coarse-Grained Models. *The Journal of Physical Chemistry C*. (doi:10.1021/acs.jpcc.6b12148).
- [70] Bussi, G., Donadio, D. & Parrinello, M. 2007 Canonical sampling through velocity rescaling. *The Journal of Chemical Physics* **126**, 014101. (doi:10.1063/1.2408420).
- [71] Berendsen, H.J.C., Postma, J.P.M., Gunsteren, W.F.v., DiNola, A. & Haak, J.R. 1984 Molecular dynamics with coupling to an external bath. *The Journal of Chemical Physics* **81**, 3684-3690. (doi:10.1063/1.448118).
- [72] Baoukina, S., Marrink, S.J. & Tieleman, D.P. 2010 Lateral pressure profiles in lipid monolayers. *Faraday Discuss* **144**, 393-409. (doi:10.1039/b905647e).
- [73] Choe, S., Chang, R., Jeon, J. & Violi, A. 2008 Molecular dynamics simulation study of a pulmonary surfactant film interacting with a carbonaceous nanoparticle. *Biophysical Journal* **95**, 4102-4114. (doi:10.1529/biophysj.107.123976).
- [74] Humphrey, W., Dalke, A. & Schulten, K. 1996 VMD: Visual molecular dynamics. *Journal of Molecular Graphics* **14**, 33-38. (doi:10.1016/0263-7855(96)00018-5).
- [75] Baoukina, S., Monticelli, L., Marrink, S.J. & Tieleman, D.P. 2007 Pressure–Area Isotherm of a Lipid Monolayer from Molecular Dynamics Simulations. *Langmuir* **23**, 12617-12623. (doi:10.1021/la702286h).

LIST OF TABLE

Table 1. Summary of the simulation systems with 651 DPPC, 279 POPG and 93 cholesterol molecules per monolayer. The water thickness was 21 nm between two monolayers, and the temperature was at 310 K.

AuNP concentrations (mol %)	No. of AuNPs in each monolayer	APL nm ²	Pore formation
~0.1	1	0.46	No
		0.53	No
~0.9	9	0.46	No
		0.53	No
~1.56	16	0.46	No
		0.53	No
~3.52	36	0.46	Yes
		0.53	Yes